Chemical Science

ROYAL SOCIETY OF CHEMISTRY

EDGE ARTICLE

View Article Online
View Journal | View Issue



Cite this: *Chem. Sci.*, 2025, **16**, 18852

All publication charges for this article have been paid for by the Royal Society of Chemistry



# Color-tunable ultralong room temperature afterglow in a wide excitation range from ultraviolet to visible light *via* doping boric acid with polyaromatic hydrocarbons

Siyu Yan,†[a] Yunze Huang,†[b] Weibo Zhang,[a] Hongpu Xin,[a] Jing Yang[c] and Peng Li *[a]

Received 24th June 2025
Accepted 8th September 2025

DOI: 10.1039/d5sc04627k

rsc.li/chemical-science

The development of ultralong organic room temperature afterglow (UL-RTA) materials has attracted tremendous attention owing to their great potential applications in optoelectronic areas. However, achieving UL-RTA, particularly under visible-light activation, remains a substantial challenge. Herein, we present an effective strategy to achieve excitation wavelength-dependent UL-RTA behavior covering a wide range from ultraviolet (UV) to the visible light region *via* embedding polycyclic aromatic hydrocarbons (PAHs containing triphenylene (TP) and coronene (CN)) into a boric acid (BA) matrix (denoted as PAHs-BA, TP-BA and CN-BA). Specifically, the TP-BA system exhibits a minute-level blue UL-RTA with an ultralong lifetime of 6744 ms, while the CN-BA system demonstrates a green afterglow with an ultralong lifetime of 3724 ms lasting up to 25 s under visible light excitation at 420 nm. Such outstanding afterglow performance has been rarely reported so far. Experiments and theoretical calculations indicate that the observed UL-RTA primarily originates from the rigid and confined environment provided by the formation of a metaboric acid (HBA) matrix under heat treatment, which effectively suppresses non-radiative transitions of the guest molecules. Furthermore, the excitation-dependent performance covering a wide range from UV to the visible light region mainly relies on the coexistence of the isolated individuals and J-aggregation of guest molecules. Inspired by these outstanding features, anti-counterfeiting and multilevel information encryption applications are demonstrated.

## 1 Introduction

Organic room temperature afterglow (RTA) materials have attracted tremendous attention in optoelectronic areas ranging from sensing, anti-counterfeiting, and information encryption to optoelectronic devices and biological imaging due to their long lifetime, large Stokes shifts, high exciton utilization and rich excited state properties.[1–8] As they rely on the generation of triplet excitons, the following strategies are crucial to achieve effective RTA emission that is promoting the intersystem crossing (ISC) process from the lowest excited singlet state ($S_1$) to triplet states ($T_n$) by enhancing spin–orbit coupling (SOC) and/or suppressing the nonradiative decay of triplet excitons *via* inhibiting molecule vibration.[9,10] In this regard, many excellent strategies have been proposed in recent years, such as host–guest complexation, crystallization engineering, integration with heavy/hetero-atoms and doping in polymers, *etc.*[11–20] However, to date, the afterglow lifetimes ($\tau_{Afterglow}$), quantum yields ($\Phi_{Afterglow}$) and color diversity of many afterglow materials are not satisfactory.[21–23] Moreover, most of the reported afterglow systems can only be activated by UV light, limiting their widespread practical applications.[24–26] As far as we know, visible light is safer, healthier, more penetrating, and has more practical applications in multiple areas especially biological and life applications.[27–30] Hence, it is urgently necessary to develop highly efficient afterglow systems with wide-range excitation including visible light.

It is noteworthy that PAHs with large conjugated planar and rigid chemical structures are conducive for suppressing non-radiative transitions by reducing molecular vibrations. Furthermore, these compounds have the capacity to achieve a redshift in absorption or excitation wavelengths through controlled aggregation or modulation of the degree of conjugation.[31,32] Meanwhile, their singlet and triplet excited-state energy levels are highly sensitive to variations in the chemical

[a]*Tianjin Key Laboratory of Chemical Process Safety, Hebei Key Laboratory of Functional Polymers, School of Chemical Engineering and Technology, Hebei University of Technology, Tianjin, 300401, PR China. E-mail: lipeng@hebut.edu.cn*

[b]*Beijing Advanced Innovation Center for Soft Matter Science and Engineering, State Key Laboratory of Chemical Resource Engineering, College of Materials Science and Engineering, Beijing University of Chemical Technology, Beijing 100029, PR China*

[c]*School of Resources & Chemical Engineering, Sanming University, Sanming, 365004, Fujian, PR China*

† These authors contributed equally.

structure, offering the possibility of obtaining efficient afterglow emission with tunable color.[33,34] In recent years, several bright afterglow systems with an ultralong lifetime have been realized by embedding PAHs into polymer matrices. However, most of them exhibit only a single afterglow color and are usually limited to UV light excitation.[35,36] Consequently, achieving efficient afterglow emission with tunable color in a broad excitation range, including visible light, remains challenging.

Inorganic boric acid (BA) as a host matrix could effectively suppress the molecular vibration- and rotation-assisted nonradiative decay due to its high degree of rigidity[37,38] BA can also form a through-space conjugation (TSC) structure in the B–O confined space because of its empty p-orbital and electron-accepting capability,[39,40] thus providing the confinement environment for guest molecules. These advantages provide possibility for the ordered aggregation formation of guest molecules and the regulation of conjugation degree, which is promising for the achievement of multiple afterglow color with visible light-excitation.[41–43] So far, a few bright afterglow systems using boronic acid as the host matrix and aromatic compounds as the guest have been reported.[44–47] Although some of them show ultralong lifetime up to 8.74 s, some of them display ultrahigh quantum yield up to 57.66%. However, a vast majority of them present only single afterglow color and are usually limited to UV light excitation.

Herein, TP and CN molecules were selected as the guest molecules and embedded into a BA matrix to achieve color-tunable afterglow behavior with excitation wavelength-dependent feature covering a wide range from UV to the visible light region (denoted as TP-BA and CN-BA). Remarkably, benefiting from the unique HBA rigid and confined microenvironment generated after heating, the TP-BA system shows a duration of up to 65 s excited at 254 nm, with an ultralong lifetime of 6744 ms. More impressively, the CN-BA system demonstrates green afterglow emission lasting up to 25 s with an ultralong lifetime of 3724 ms and an afterglow quantum yield of 11.06% upon visible light excitation of 420 nm. The experimental data further reveal that the coexistence of isolated individuals and aggregation states of guest molecules is the key to achieving broad excitation wavelength dependence. Inspired by these unique properties, anti-counterfeiting and multilevel information encryption applications are achieved.

## 2 Results and discussion

Two kinds of UL-RTA systems were fabricated *via* embedding TP and CN into a BA matrix using a solid phase heat treatment method at 200 °C (Fig. 1a). Intriguingly, the PAHs-BA systems exhibit excitation wavelength-dependent afterglow behavior covering a wide range from UV to the visible light region. As depicted in Fig. 1b, c and SI Movie 1, the afterglow emission color of TP-BA systems changed from blue to green, when the excitation wavelength changed from 254 to 420 nm. Importantly, blue afterglow excited at 254 nm can show duration times up to 65 s. Even though the excitation wavelength is up to 420 nm, it is still capable of emitting green afterglow with a duration time of about 10 s. As displayed in Fig. 1c, CN-BA systems display not very obvious tunable afterglow color from yellow to green when switching off the excitation source from 254 to 420 nm. Impressively, the green afterglow upon excitation at 420 nm exhibits duration times up to 25 s (Fig. 1c), which is rarely seen so far.

To investigate this interesting afterglow phenomenon, the afterglow spectra of TP-BA and CN-BA systems with different excitation wavelengths were measured. When the excitation wavelength is in the range from 254 to 340 nm, the afterglow emission spectra of TP-BA display four peaks at 440, 465, 493, and 534 nm (Fig. 2a), with Commission International de lEclairage (CIE) chrominance coordinates of (0.16, 0.19). As depicted in Fig. 2b, when the excitation wavelength ranges from 340 to 440 nm, the relative intensity of blue and green emissions rapidly decreases, while that of orange and red emissions increases, accompanied by a change in their CIE chrominance coordinates from (0.16, 0.19) to (0.39, 0.49). Additionally, TP-BA displays an ultralong lifetime of 6.50, 6.74, 2.33, 0.35 s fitted by a double exponential function according to the following equation (eqn (1)) and (Table S1)[48,49] with the longest $\tau_{Afterglow}$ up to 6744 ms and an afterglow quantum yield of 23.2%, 11.9%, 15.0%, and 10% under excitation from 254 to 420 nm (Fig. 2c and Table S2). Meanwhile, the CN-BA system exhibited increasing blue emission at 515 and 533 nm and decreasing green emission at 565 nm with CIE chrominance coordinates ranging from (0.42, 0.54) to (0.36, 0.51), as the excitation wavelength changes from 254 to 420 nm (Fig. 2d and e). And this system displays a lifetime of 4.04, 4.02, and 3.56 s and an afterglow quantum yield of 2.04%, 24.12%, and 4.05% upon excitation at 254, 310 and 365 nm (Fig. 2f and Table S3), respectively. Surprisingly, this system reveals an ultralong lifetime of 3724 ms and an afterglow quantum yield of 11.06% upon visible light excitation of 420 nm (Table S2). To the best of our knowledge, afterglow materials with $\tau_{Afterglow}$ over 4.5 s under UV light and $\tau_{Afterglow}$ over 2.1 s under visible light have not been reported to date. These interesting results will create new opportunities for their application in the fields of anti-counterfeiting and multilevel information encryption.

$$\tau_{avg} = \sum \alpha_i \tau_i^2 / \sum \alpha_i \tau_i \quad (1)$$

To explore the afterglow mechanism of PAHs-BA systems, a series of TP-BA samples as models were prepared at different reaction temperatures for comparative experiments (named TP-BA@$x$ °C). We discovered that TP-BA before heat treatment exhibits no obvious afterglow behaviors (Fig. S1), which start to show weak afterglow emission excited at 254 nm at a heat treatment temperature of 150 °C. When the heat treatment temperature increased to 200 °C, TP-BA displays excellent afterglow properties as mentioned above. As the temperature further increases to 250 °C and 300 °C, the decrease in afterglow characteristics can be found (Fig. S2 and S3). To explore the reason for this phenomenon, their X-ray diffraction (XRD) pattern and thermogravimetric (TGA) curves were measured using TP-BA as models. As illustrated in Fig. 3a, both TP-BA

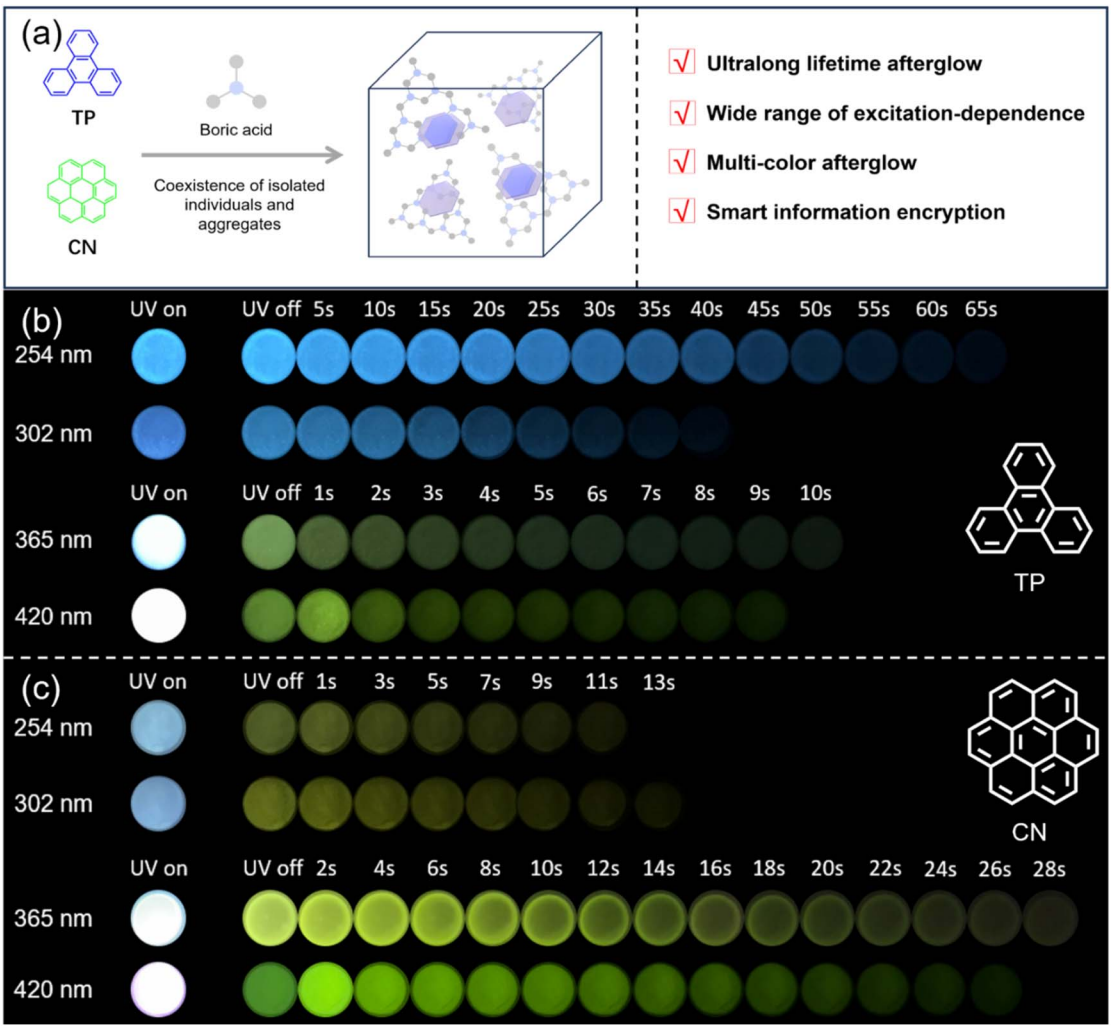


Fig. 1 (a) Schematic diagram of the synthetic process and structure of PAHs-BA; digital photos of (b) TP-BA and (c) CN-BA before and after turning off UV light at different excitation wavelengths and 420 nm visible light.

before heat treatment and TP-BA@150 °C mainly display a sharp diffraction peak at about 28° belonging to the (100) plane, suggesting the triclinic phase of BA.[50] However TP-BA@200 °C exhibits a sharp peak at near 28.9° and several small peaks at 16.5, 20.2 and 25.0°, which are consistent with the characteristic peaks of HBA, demonstrating the formation of HBA.[51,52] As the reaction temperature increases to 250 and 300 °C, XRD reveals the presence of the characteristic peak associated with boron oxide. At this time, the crystallinity of the sample is reduced, accompanied by a transition to a glassy state.[53,54] Additionally, the TGA curve reveals that the weight of BA drops sharply to 70% of the initial weight and tends to balance, which is consistent with the dehydration process of BA into metaboric acid with the temperature increasing from 100 to 150 °C (Fig. 3b). As the temperature further increases from 200 to 400 °C, the weight of BA slowly decreases, implying further dehydration of BA and the formation of boron oxide.[55] These results suggest the important role of the HBA matrix in the generation of the above-mentioned excellent afterglow behaviors (Fig. S4).

To further verify the positive effects of the HBA matrix on promoting the afterglow generation for TP-BA, Fourier transform infrared (FTIR) spectroscopy and scanning electron microscopy (SEM) were performed. As displayed in Fig. 3c, the FTIR spectrum of HBA shows the absorption peaks located at 650 and 805 $cm^{-1}$ attributed to the deformation vibrations of the B–O bonds and B–OH bonds, respectively, and the peak of 1400 $cm^{-1}$ with a shoulder related to the vibration of atoms in the B(III)–$O^-$ bond.[52,55] TP-BA has an almost identical FTIR spectrum to HBA, and their absorption peaks have no obvious shift. This fact demonstrates that there is no hydrogen bond interaction between TP and HBA. Scanning electron microscopy (SEM) of TP-BA reveals denser and crystallized particles with an irregular shape compared with that of BA (Fig. 3d–g). Therefore, we infer that the HBA matrix provides a tight and rigid environment for TP molecules to suppress their nonradiative transitions through preventing their vibrational and rotational motion.

To gain an in-depth insight into the foregoing interesting tunable afterglow color of TP-BA with excitation-dependent

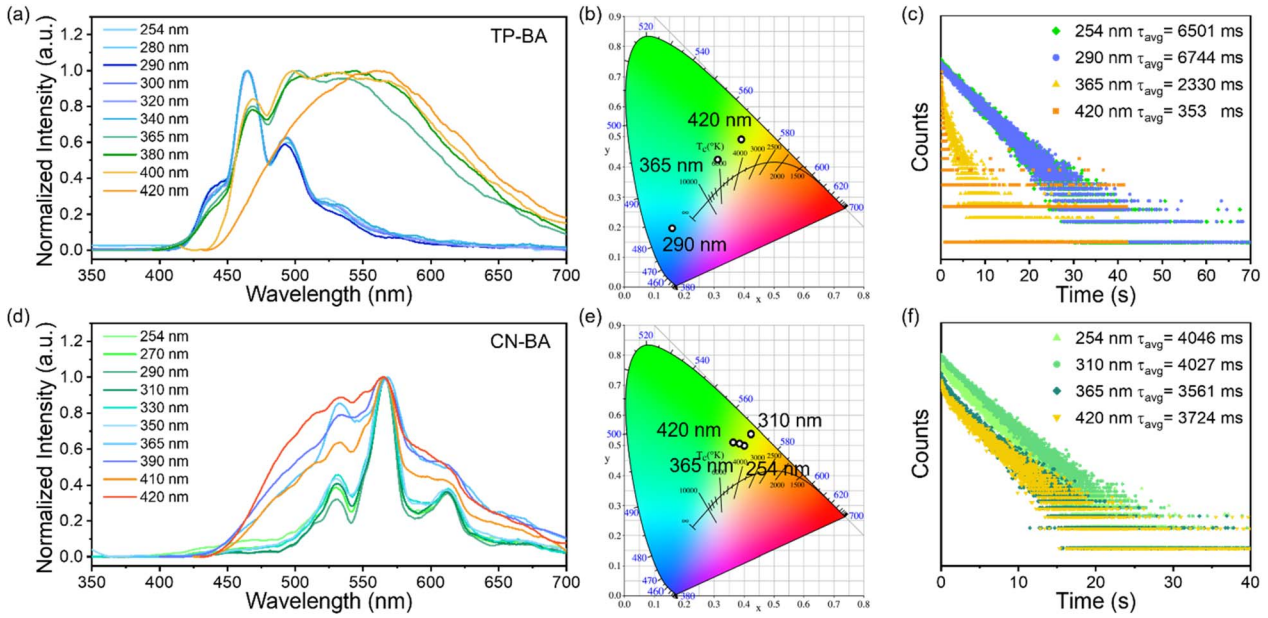


Fig. 2 (a) Normalized delayed emission spectra; (b) CIE chromaticity coordinates and (c) delayed emission decay curves of TP-BA excited at different excitation wavelengths; (d) normalized delayed emission spectra; (e) CIE chromaticity coordinates and (f) delayed emission decay curves of CN-BA excited at different excitation wavelengths.

performance covering a wide range from UV to the visible light region, a series of comparative tests were conducted. First, we compare the afterglow emission spectra of TP-BA and TP dilute solutions of $10^{-5}$ mol $L^{-1}$ and $10^{-4}$ mol $L^{-1}$ at 77 K. TP dilute solutions of $10^{-5}$ mol $L^{-1}$ display multiple afterglow emission peaks at 430 to 500 nm with the optimal emission peak at 465 nm under high-energy excitation of 254, 290 and 365 nm, while the relative intensity of blue and green emissions at 430 to 500 nm significantly decreases, and that of orange and red emissions at 620 to 700 nm increases upon excitation at 420 nm (Fig. S5). As the concentration increases to $10^{-4}$ mol $L^{-1}$, TP dilute solutions show a similar afterglow emission upon excitation of 254 and 290 nm. However, the relative intensity of blue and green emissions at 465 nm significantly decreases, while the emission band in orange and red regions at 500 to 600 nm accounts for the absolute dominant position upon excitation of 365 and 420 nm (Fig. S6). These results indicate that the blue and green emissions at 465 nm are related to the isolated individuals, while the orange and red regions at 500 to 600 nm belong to the aggregation state. Additionally, TP-BA systems

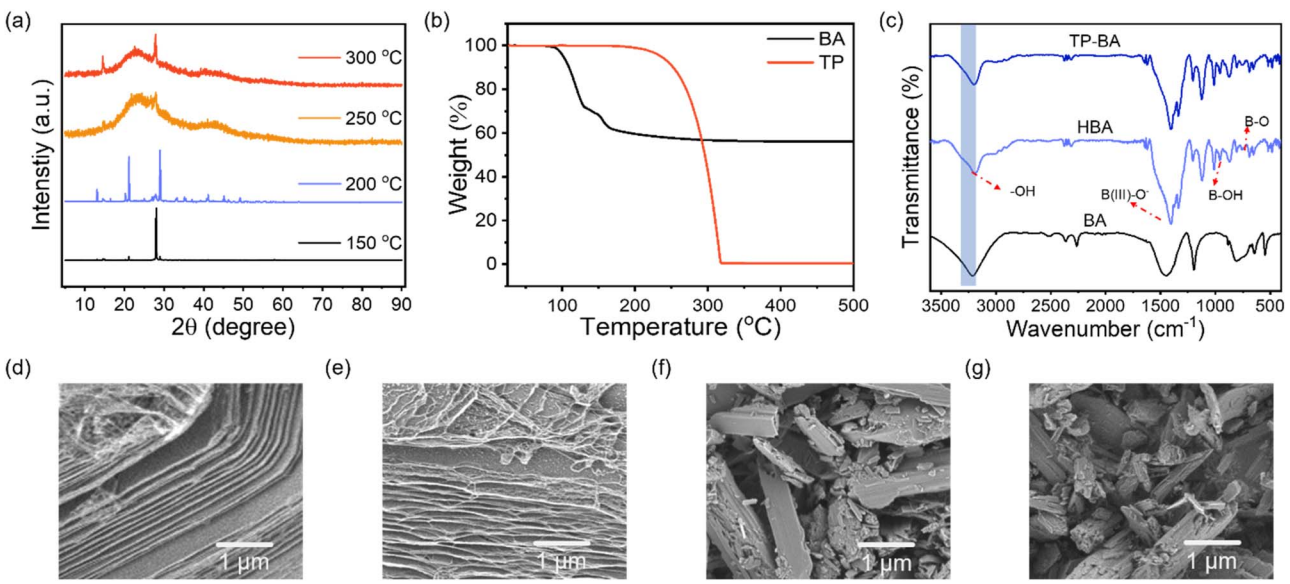


Fig. 3 (a) XRD patterns of TP-BA at different reaction temperatures; (b) TGA curves of TP and BA; (c) FT-IR spectra of BA, HBA and TP-BA; SEM images of (d) BA; (e) TP and BA before heating; (f) HBA and (g) TP-BA.

with different doping contents of TP display similar changing trends (Fig. S7 and S8). Notably, TP-BA reveals similar afterglow emission spectra to that of TP dilute solutions of $10^{-4}$ mol $L^{-1}$ at various excitation wavelengths (Fig. S6), demonstrating the coexistence of the isolated individuals and aggregation in TP-BA systems, which also can be supported by the redshifted absorption band and the new emerging absorption band relative to that for TP dilute solutions at a concentration of $10^{-5}$ mol $L^{-1}$ in their UV-vis absorption spectra (Fig. S9).[56,57] Similarly, the absorption peaks of the TP crystal also display an obvious redshift (containing the visible light region) compared with those of TP dilute solutions at a concentration of $10^{-5}$ mol $L^{-1}$ (Fig. S10), suggesting the presence of J-aggregation.[35] To further verify the above-mentioned inference, the single crystal structures of TP were determined to analyze the molecular conformation. As shown in Fig. 4a, the crystals of TP are assigned to the $P2_12_12_1$ space group, wherein the molecules are stacked in parallel and partially face-to-face with a distance of 3.372 Å. The angle between the molecular transition dipoles and the interconnecting axis ($\theta$) is 39.801°, which is less than the critical value of 54.7 for distinction of H- and J-aggregation, testifying the presence of J-aggregation in the crystal.[58,59] Additionally, BA@200 °C (BA upon heat treatment at 200 °C) also has afterglow behaviors upon various excitation ranging from 254 nm to 420 nm (Fig. S11), yet which is similar to that of TP-BA only when the excitation wavelength is greater than 365 nm. This may be due to too weak afterglow emission intensity under excitation at less than 365 nm (Fig. S12). Moreover, the afterglow emission intensities of BA@200 °C are weaker than those of TP-BA, which may be because the formation of the conjugated system with n or $\pi$ transitions *via* the vacant p orbitals on the boron atom promotes the ISC efficiency. This result can be supported by the obvious peaks with a *g*-factor of 2.002 in the EPR spectra of BA@200 °C (Fig. S13).[52] Based on the above data, we deduce that the foregoing interesting excitation-dependent performance covering a wide range from UV to the visible light region of TP-BA is induced by the coexistence of the isolated individuals and aggregation of TP molecules and the minor contribution of BA@200 °C. It is noteworthy that these systems of employing LAPONITE® (Lap) and Amino clay (AC) as matrices through the same procedures exhibit no obvious afterglow behaviors (Fig. S14), which suggests the important role of the BA matrix in the generation of the above-mentioned afterglow phenomenon. This may be because both Lap and AC are layered inorganic host materials, presenting looser structures.[60,61]

To further understand the relationship between the coexistence of the isolated individuals and aggregation of TP molecules and the excitation-dependent afterglow emission behavior, we determined the singlet and triplet energy levels of TP-BA by theoretical calculations using the density functional theory (DFT) method. As depicted in Fig. 4b and Table S4–S7, in the monomer state, the ISC from singlet to triplet states has limited ISC routes. As the increasing aggregation content (such as from the dimer to trimer), the energy levels of the emission excited states have a tendency to converge as a result of the significant decrease in the energy difference between $S_n$ ($n > 1$) and $S_1$ [and between $T_n$ ($n > 1$) and $T_1$], which supply more and efficient ISC pathways at upper triplet levels. This trend is the essence for the regulation of the afterglow emission from variable triplet states, thus achieving the excitation-dependent afterglow emission behavior in TP-BA systems.[62,63]

Inspired by the unique excitation-wavelength-dependent afterglow characteristic of TP-BA and CN-BA, diverse encryption patterns were developed to exhibit their potential applications in advanced anti-counterfeiting technology. As illustrated in Fig. 5a, the letters "H B T" and "E U" are drawn by TP-BA and CN-BA, respectively. The letters "H B T" and "E U" display blue and green fluorescence upon UV irradiation at 254 nm and 302 nm, which turns into blue and green afterglow, respectively, after removing the UV light irradiation. Owing to the longer afterglow lifetime of letters "H B T", the original word "HEBUT" turns into the new word "HBT" with blue afterglow successively after ceasing the UV light irradiation for 30 s. Unlike this, when the irradiation source changed from 254 and 302 nm to 365 and 420 nm, the letters "H B T" and "E U" show similar green luminescence and afterglow. Over time, only the letters "E U" remain and can be identified owing to their longer afterglow. Therefore, multilevel information encryption can be achieved making use of the excitation wavelength-responsive afterglow nature of PAHs-BA systems. Except for the letter encryption, tailor-made patterns such as 'two-dimensional code (QR code)'

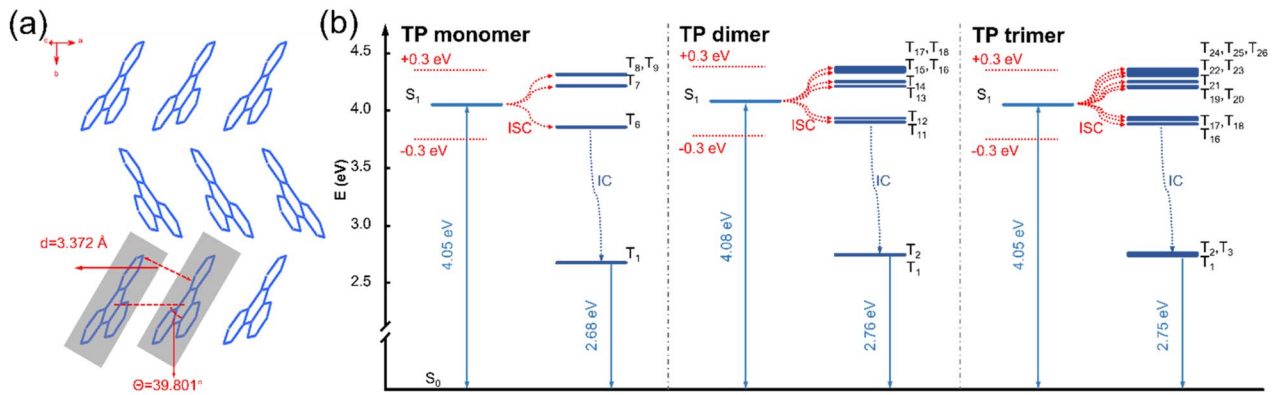


Fig. 4 (a) Single-crystal structures of isolated individuals of TP and (b) DFT calculations of energy levels of the TP monomer, dimer and trimer.

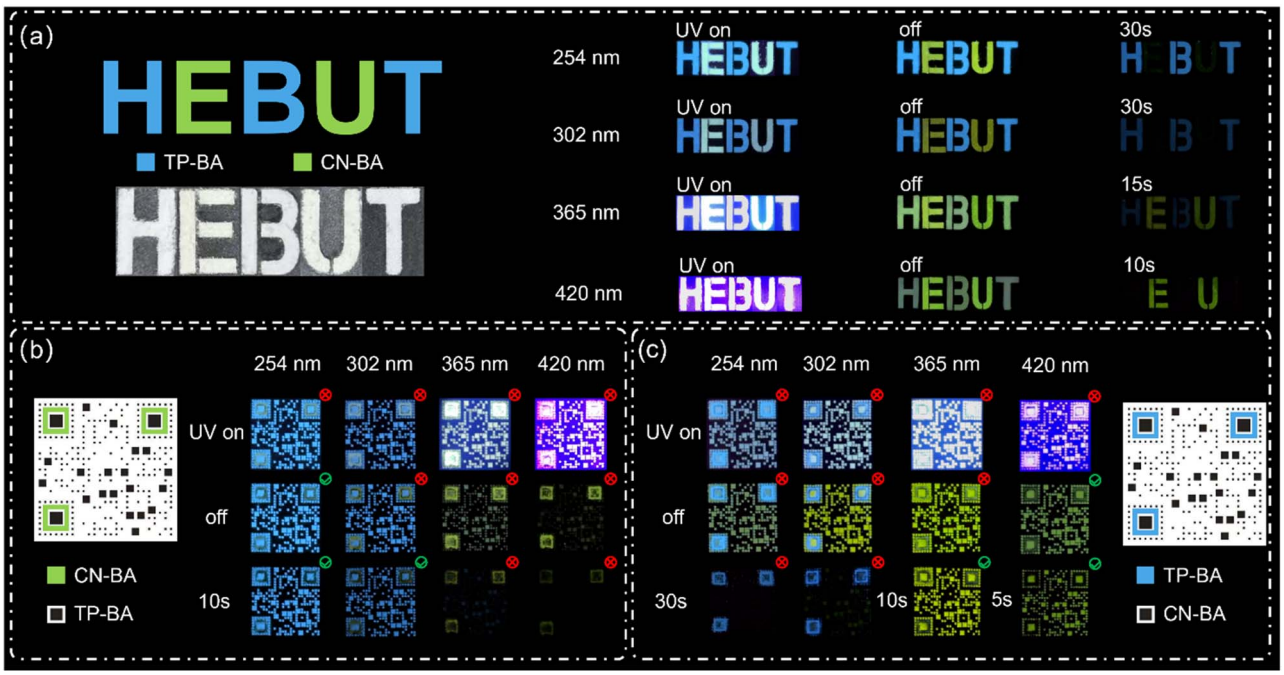


Fig. 5 PAHs-BA is used in anti-counterfeiting and information encryption: (a) digital images of information encryption patterns prepared by TP and CN under different excitation light sources; (b) and (c) digital photos of multi-stage information encryption QR code patterns prepared by TP-BA and CN-BA at different excitation light wavelengths.

are also fabricated to enrich the diversity of the encryption mode. Two QR codes with implicit information of the official website for "the College of Chemical Engineering of Hebei University of Technology" were designed utilizing TP-BA and CN-BA (Fig. 5b and c). As displayed in Fig. 5b, the black body region of the QR code was made of TP-BA, while three green corners were covered by CN-BA. Under irradiation at 254, 302, 365 and 420 nm, the QR code cannot be recognized to provide any information as a result of the partially covered identification division. Interestingly, a recognizable QR code was first obtained upon turning off UV light of 254 nm, which turns out to be a recognized pattern with time elapsing after switching of the UV lamp of 302 nm because of the longer afterglow of TP-BA, while the QR code has never been recognized after ceasing the irradiation source of 365 and 420 nm thanks to the longer afterglow of CN-BA. In contrast, the black body region and three green corners of the QR code were covered by CN-BA and TP-BA, which can acquire the extremely different result. As displayed in Fig. 5c, the recognizable QR code can be achieved by removing the irradiation of 365 and 420 nm, while the QR code is unrecognizable after turning off the UV light irradiation of 254 and 302 nm. These results demonstrate that the as-prepared interesting excitation-dependent afterglow performance of PAHs-BA systems has important potential applications in advanced anti-counterfeiting technology.

## 3 Conclusions

In summary, we report an effective strategy to achieve excitation wavelength-dependent afterglow behavior covering a wide range from UV to the visible light region *via* embedding PAHs (TP and CN) into a BA matrix. Importantly, the blue afterglow of TP-BA can show duration times up to 65 s when excited at 254 nm, displaying an ultralong lifetime of 6744 ms. More impressively, the green afterglow of CN-BA exhibits duration times up to 25 s with an ultralong lifetime of 3724 ms and an afterglow quantum yield of 11.06% upon visible light excitation of 420 nm. Such outstanding afterglow characteristics have been rarely seen so far. It is found that the HBA matrix generated after heating BA plays an important role in the generation of the above-mentioned excellent afterglow behaviors. A series of control experiments and theoretical calculations demonstrate that the HBA matrix provides a tight and rigid environment for guest molecules to suppress their nonradiative transitions through preventing their vibrational and rotational motion. Additionally, their interesting excitation-dependent performance covering a wide range from UV to the visible light region is attributed to the coexistence of the isolated individuals and J-aggregation of guest molecules supplying more efficient ISC pathways and the minor contribution of BA@200 °C. Given these outstanding features, their applications in the field of anti-counterfeiting and multilevel information encryption are exploited. This points out a promising research direction for the development of color tunable RTA materials with excitation-dependent performance covering a wide range from UV to the visible light region toward practical applications in high precision anti-counterfeiting and information encryption. This work is expected to serve as a valuable guide for designing color-tunable afterglow materials with excitation wavelength-dependent feature covering a wide range from UV to the visible light region.

## Author contributions

Y. Z. Huang, S. Y. Yan, and P. Li conceived the idea and designed the experiments. Y. Z. Huang, S. Y. Yan and W. B. Zhang performed the experiments and characterized the hybrid films. Y. Z. Huang and S. Y. Yan wrote the paper with support from P. Li. All authors reviewed and edited the manuscript.

## Conflicts of interest

There are no conflicts to declare.

## Data availability

The data that support the findings of this study are available from the corresponding author upon reasonable request.

Supplementary information is available. See DOI: **https://doi.org/10.1039/d5sc04627k**.

## Acknowledgements

Financial support from the National Natural Science Foundation of China (22405070 and 22305061 (C0057048)), Hebei Natural Science Foundation (B2022202032 and E2022402061), and the Hebei Provincial College of Science and Technology Research Project (BJ2018054) is acknowledged.

## Notes and references

1 N. Y. Li, X. P. Yang, B. B. Wang, P. Y. Chen, Y. X. Ma, Q. Q. Zhang, Y. Y. Huang, Y. Zhang and S. Y. Lv, *Adv. Sci.*, 2024, **11**, 2404698.
2 Z. Q. Yang, H. C. Liu, X. Y. Zhang, Y. B. Lv, Z. Y. Fu, S. Q. Zhao, M. Liu, S. T. Zhang and B. Yang, *Adv. Mater.*, 2024, **36**, 2306784.
3 L. Y. Liang, B. B. Chen, Y. T. Gao, J. Lv, M. L. Liu and D. W. Li, *Adv. Mater.*, 2024, **36**, 2308180.
4 J. J. Shi, W. J. Tao, Y. S. Zhou, P. Zhang and G. D. Liang, *Chem. Eng. J.*, 2024, **498**, 155737.
5 S. Y. Zong, X. W. Yu, Y. N. Yang, X. Yang and J. Y. Li, *Chin. Chem. Lett.*, 2025, **36**, 110343.
6 G. Li, J. Pu, Z. Yang, H. Deng, Y. Liu, Z. Mao, J. Zhao, S. J. Su and Z. Chi, *Aggregate*, 2023, **4**, e382.
7 J. J. Shi, Y. S. Zhou, W. Wang, Z. Y. Yang, P. Zhang and G. D. Liang, *Chem. Eng. J.*, 2024, **492**, 152419.
8 Y. Y. Zhao, J. H. Yang, C. Liang, Z. J. Wang, Y. F. Zhang, G. C. Li, J. M. Qu, X. Wang, Y. H. Zhang, P. Sun, J. B. Shi, B. Tong, H. Y. Xie, Z. X. Cai and Y. P. Dong, *Angew. Chem., Int. Ed.*, 2024, **63**, e202317431.
9 Q. Jia, X. Yan, B. Wang, J. Li, W. Xu, Z. Shen, C. Bo, Y. Li and L. Chen, *Nat. Commun.*, 2023, **14**, 4164.
10 Z. Wang, J. J. Liu, M. Y. Li and G. Chen, *Chem. Eng. J.*, 2023, **462**, 142154.
11 H. D. Guo, M. N. Cao, R. X. Liu, B. Tian, S. X. Liu, J. Li, S. J. Li, B. Strehmel, T. D. James and Z. J. Chen, *Nat. Commun.*, 2024, **15**, 1590.
12 L. L. Wei, F. R. Gao, C. He, Q. H. He, P. Y. Jin, Y. Q. Rong, T. Zhao, C. Yang and W. H. Wu, *Sci. China Chem.*, 2023, **66**, 3546–3554.
13 J. S. Xiao, J. W. Deng, X. S. Wang, H. L. Ho, C. H. Bai, Y. H. Bai and H. L. Wang, *Small*, 2024, **20**, 2405615.
14 B. Chen, W. H. Huang and G. Q. Zhang, *Nat. Commun.*, 2023, **14**, 1514.
15 Z. C. Cheng, H. F. Shi, H. L. Ma, L. F. Bian, Q. Wu, L. Gu, S. Z. Cai, X. Wang, W. W. Xiong, Z. F. An and W. Huang, *Angew. Chem., Int. Ed.*, 2017, **57**, 678–682.
16 W. P. Ye, H. L. Ma, H. F. Shi, H. Wang, A. Q. Lv, L. F. Bian, M. Zhang, C. Q. Ma, K. Ling, M. X. Gu, Y. F. Mao, X. K. Yao, C. F. Gao, K. Shen, W. Y. Jia, J. H. Zhi, S. Z. Cai, Z. C. Song, J. J. Li, Y. Y. Zhang, S. Lu, K. Liu, C. M. Dong, Q. Wang, Y. D. Zhou, W. Yao, Y. J. Zhang, H. M. Zhang, Z. Y. Zhang, X. C. Hang, Z. F. An, X. G. Liu and W. Huang, *Nat. Mater.*, 2021, **20**, 1539–1544.
17 G. Y. Liu, L. T. Yue, Y. G. Wang, S. F. Xue, Q. K. Sun and W. J. Yang, *Chem. Eng. J.*, 2024, **498**, 155171.
18 S. H. Sun, Q. Fu, Z. H. Dong and M. B. Yue, *Chem. Eng. J.*, 2024, **499**, 155972.
19 Q. Q. Xia, X. H. Wang, J. L. Yu, Z. Y. Chen, X. Y. Lou, X. Liu, M. X. Wu and Y. W. Yang, *Aggregate*, 2023, **4**, e370.
20 Y. Yang, J. Wang, J. Yang, L. Tong, D. Li, Y. Yang, M. Fang and Z. Li, *Angew. Chem., Int. Ed.*, 2023, **62**, e202218994.
21 Q. Y. Liao, Q. H. Gao, J. Q. Wang, Y. B. Gong, Q. Peng, Y. Tian, Y. Y. Fan, H. J. Guo, D. Ding, Q. Q. Li and Z. Li, *Angew. Chem., Int. Ed.*, 2020, **59**, 9946–9951.
22 W. J. Guo, S. R. Yan, L. Chen, L. Qiao, S. H. Xu, T. F. Qi, B. Liu and H. Q. Peng, *Adv. Funct. Mater.*, 2024, **34**, 2406888.
23 Y. H. Xu, Y. Zhu, L. Q. Kong, S. C. Sun, F. Li, F. R. Tao, L. P. Wang and G. Li, *Chem. Eng. J.*, 2023, **453**, 139753.
24 K. Y. Chen, Y. Xiong, D. L. Wang, Y. W. Pan, Z. Zhao, D. Wang and B. Z. Tang, *Adv. Funct. Mater.*, 2024, **34**, 2312883.
25 S. Y. Zong, J. N. Zhang, X. Yin, J. Y. Li and S. N. Qu, *Nano Lett.*, 2024, **24**, 1859–1866.
26 Q. Yao, Y. Wang, M. Q. Wang, N. V. Gaponenko, Z. Da, J. D. Shi, C. Zhang and J. N. Wang, *Mater. Today Chem.*, 2024, **40**, 102199.
27 Y. Y. Fan, S. W. Liu, M. Wu, L. Y. Xiao, Y. H. Fan, M. M. Han, K. Chang, Y. F. Zhang, X. Zhen, Q. Q. Li and Z. Li, *Adv. Mater.*, 2022, **34**, 2201280.
28 H. L. Wu, Y. X. Kang, S. N. Jiang, K. T. Wang, L. J. Qu and C. L. Yang, *Small*, 2024, **20**, 2402796.
29 Y. Zheng, Z. H. Wang, J. W. Liu, Y. F. Zhang, L. Gao, C. Wang, X. Zheng, Q. Zhou, Y. Yang, Y. B. Li, H. L. Tang, L. J. Qu, Y. L. Zhao and C. L. Yang, *ACS Appl. Mater. Interfaces*, 2022, **14**, 15706–15715.
30 L. Q. Li, D. P. Liu, J. Y. Zhou, M. Qi, G. Q. Yin and T. Chen, *Mater. Horiz.*, 2024, **11**, 5895–5913.
31 J. Mei, N. L. C. Leung, R. T. K. Kwok, J. W. Y. Lam and B. Z. Tang, *Chem. Rev.*, 2015, **115**, 11718–11940.
32 F. M. Xiao, H. Q. Gao, Y. X. Lei, W. B. Dai, M. C. Liu, X. Y. Zheng, Z. X. Cai, X. B. Huang, H. Y. Wu and D. Ding, *Nat. Commun.*, 2022, **13**, 186.

33 Y. Xia, C. F. Zhu, F. Cao, Y. X. Shen, M. Ouyang and Y. J. Zhang, *Angew. Chem., Int. Ed.*, 2023, **62**, e202217547.
34 J. Y. Liang, J. Yang, Y. S. Wang, M. D. Shan, Z. J. Liu, J. Ren, M. M. Fang and Z. Li, *Sci. China Mater.*, 2024, **67**, 2778–2788.
35 X. X. Zheng, Q. X. Han, Q. L. Lin, C. C. Li, J. K. Jiang, Q. Guo, X. Ye, W. Z. Yuan, Y. Liu and X. T. Tao, *Mater. Horiz.*, 2023, **10**, 197–208.
36 Y. H. Liang, P. T. Hu, H. Q. Zhang, Q. C. Yang, H. S. Wei, R. T. Chen, J. H. Yu, C. Liu, Y. H. Wang, S. L. Luo, G. Shi, Z. G. Chi and B. J. Xu, *Angew. Chem., Int. Ed.*, 2024, **63**, e202318516.
37 Z. Wu, J. C. Roldao, F. Rauch, A. Friedrich, M. Ferger, F. Würthner, J. Gierschner and T. B. Marder, *Angew. Chem., Int. Ed.*, 2022, **61**, e202200599.
38 J. Gierschner, J. Shi, B. Milián-Medina, D. Roca-Sanjuán, S. Varghese and S. Y. Park, *Adv. Opt. Mater.*, 2021, **9**, 2002251.
39 H. Y. Zheng, P. S. Cao, Y. Y. Wang, X. M. Lu and P. Wu, *Angew. Chem., Int. Ed.*, 2021, **60**, 9500–9506.
40 Z. Zhang, Y. Shi, Y. B. Liu, Y. F. Xing, D. Yi, Z. G. Wang and D. P. Yan, *Chem. Eng. J.*, 2022, **442**, 136179.
41 X. W. Du, J. Zhou, J. F. Shi and B. Xu, *Chem. Rev.*, 2015, **115**, 11718–11940.
42 E. V. Dutrow, D. Emera, K. Yim, S. Uebbing, A. A. Kocher, M. Krenzer, T. Nottoli, D. B. Burkhardt, S. Krishnaswamy, A. Louvi and J. P. Noonan, *Nat. Commun.*, 2022, **13**, 304.
43 Y. Su, Y. F. Zhang, Z. H. Wang, W. C. Gao, P. Jia, D. Zhang, C. L. Yang, Y. B. Li and Y. L. Zhao, *Angew. Chem., Int. Ed.*, 2020, **59**(25), 9967–9971.
44 X. Zheng, Y. S. Huang, W. Lv, J. Z. Fan, Q. D. Ling and Z. H. Lin, *Angew. Chem., Int. Ed.*, 2022, **61**, e202207104.
45 S. H. Li, T. Y. Zhou, S. Y. Yang, T. W. Li, P. L. Zhang, G. Y. Li, C. Li, H. Q. Li, J. Y. Li and Q. Zhao, *Chem. Eng. J.*, 2024, **495**, 153406.
46 Z. Zhang, Z. G. Wang, X. Liu, Y. E. Shi, Z. Q. Li and Y. L. Zhao, *Adv. Sci.*, 2023, **10**, 2300139.
47 Y. F. Ding, C. Y. Yang, F. W. Gan, G. L. Zhang, C. S. Shen and H. B. Qiu, *J. Am. Chem. Soc.*, 2024, **146**, 25211–25220.
48 K. Jiang, Y. H. Wang, X. L. Gao, C. Z. Cai and H. W. Lin, *Angew. Chem., Int. Ed.*, 2018, **57**, 6216–6220.
49 W. Li, W. Zhou, Z. S. Zhou, H. R. Zhang, X. J. Zhang, J. L. Zhuang, Y. L. Liu, B. F. Lei and C. F. Hu, *Angew. Chem., Int. Ed.*, 2019, **58**, 7278–7283.
50 Y. Gao, W. Rafaniello, M. F. Toksoy, T. Munhollon and R. Haber, *RSC Adv.*, 2015, **5**, 19067–19073.
51 Z. Zhang, Z. G. Wang, X. Liu, Y. E. Shi, Z. Q. Li and Y. L. Zhao, *Adv. Sci.*, 2023, **10**, 2300139.
52 Z. Zhang, Y. E. Shi, Y. B. Liu, Y. F. Xing, D. Yi, Z. G. Wang and D. P. Yan, *Chem. Eng. J.*, 2022, **442**, 136179.
53 Y. F. Ding, C. Y. Yang, F. W. Gan, G. L. Zhang, C. S. Shen and H. B. Qiu, *J. Am. Chem. Soc.*, 2024, **146**, 25211–25220.
54 J. J. Deng, Z. H. Guan, D. L. Fu, Y. W. Zheng, Z. J. Chen, H. B. Li and X. H. Liu, *Adv. Opt. Mater.*, 2023, **11**, 2300207.
55 S. S. Hou, J. Yang and P. Li, *J. Mater. Chem. C*, 2024, **12**, 717–723.
56 Z. J. Liu, Y. Tian, J. Yang, A. S. Li, Y. S. Wang, J. Ren, M. M. Fang, B. Z. Tang and Z. Li, *Light Sci. Appl.*, 2022, **11**, 142.
57 D. M. Guo, W. Wang, K. M. Zhang, J. Z. Chen, Y. Y. Wang, T. Y. Wang, W. M. Hou, Z. Zhang, H. H. Huang, Z. G. Chi and Z. Y. Yang, *Nat. Commun.*, 2024, **15**, 3598.
58 W. Ji, B. Xue, S. Bera, S. Guerin, Y. Q. Liu, H. Yuan, Q. Li, C. Q. Yuan, L. J. W. Shimon, Q. Ma, E. Kiely, S. A. M. Tofail, M. S. Si, X. H. Yan, Y. Cao, W. Wang, R. S. Yang, D. Thompson, J. B. Li and E. Gazit, *ACS Nano*, 2020, **14**, 10704–10715.
59 X. Guo, W. L. Sheng, H. F. Pan, L. Y. Guo, H. Q. Zuo, Z. Y. Wu, S. Z. Ling, X. C. Jiang, Z. J. Chen, L. J. Jiao and E. R. Hao, *Angew. Chem., Int. Ed.*, 2024, **63**, e202319875.
60 S. Kuila, K. V. Rao, S. Garain, P. K. Samanta, S. Das, S. K. Pati, M. Eswaramoorthy and S. J. George, *Angew. Chem., Int. Ed.*, 2018, **57**, 17115.
61 R. Gao and D. P. Yan, *Chem. Sci.*, 2017, **8**, 590–599.
62 Y. C. Deng, P. Li, J. T. Li, D. L. Sun and H. R. Li, *ACS Appl. Mater. Interfaces*, 2021, **13**, 14420–14429.
63 Y. Su, Y. F. Zhang, Z. H. Wang, W. C. Gao, P. Jia, D. Zhang, C. L. Yang, Y. B. Li and Y. L. Zhao, *Angew. Chem., Int. Ed.*, 2020, **59**, 9967–9971.